Macromolecules
ARTICLE

*Macromolecules* **2011**, *44*, 719–727 **719**
DOI: 10.1021/ma102661s

# Synthesis and Characterization of Polythiophenes Bearing Aromatic Groups at the 3-Position

**Kaoru Ohshimizu,[†,⊥] Ayumi Takahashi,[†,⊥] Yecheol Rho,[‡,⊥] Tomoya Higashihara,*[,†,§] Moonhor Ree,*[,‡] and Mitsuru Ueda*[,†]**

[†]*Department of Organic and Polymeric Materials, Graduate School of Science and Engineering, Tokyo Institute of Technology, 2-12-1-H-120, O-okayama, Meguro-Ku, Tokyo 152-8552, Japan,* [‡]*Division of Advanced Materials Science, Department of Chemistry, Center for Electro-Photo Behaviors in Advanced Molecular Systems, BK School of Molecular Science, and Polymer Research Institute, Pohang University of Science & Technology (POSTECH), Pohang 790-784, Republic of Korea, and* [§]*PRESTO, Japan Science and Technology Agency (JST), 4-1-8, Honcho, Kawaguchi, Saitama 332-0012, Japan.* [⊥] *These authors equally contributed to this work*

*Received November 22, 2010; Revised Manuscript Received December 26, 2010*

ABSTRACT: Regioregular poly(3-(4′-(3″,7″-dimethyloctoxy)phenyl)thiophene) (P3PhT) and poly(3-(4′-(3″,7″-dimethyloctoxy)-3′-pyridinyl)thiophene) (P3PyT) were successfully prepared with reasonably high molecular weights and low polydispersity indices by the Grignard metathesis (GRIM) polymerization. These polymers were found to be thermally stable up to 360−390 °C, depending on the phenyl or pyridinyl linker in the bristle. Both polymer films revealed a molecularly multilayer structure (i.e., lamellar structure) whose layers stacked normal to the film plane; each lamella consists of two sublayers, namely ordered and amorphous layers. The amorphous sublayer was composed of a bilayer formed from the bristles. The ordered sublayer in P3PhT consisted of laterally stacked 3-phenylthiophene backbone chains, whereas that of P3PyT consisted of thiophene backbone chains without the pyridinyl linker. These ordered sublayer formations led a longer $\pi$-conjugation length. The enhanced $\pi$-conjugation lengths were reflected in their optical and electronic properties, showing that both P3PhT and P3PyT exhibited a lower highest occupied molecular orbital (HOMO) level and lower energy band gap compared to those of poly(3-hexylthiophene) (P3HT). Overall, the structure and properties of P3PhT and P3PyT make them promising materials for advanced polymer solar cells having an excellent performance.

## Introduction

Polythiophenes (PTs) and their derivatives have been widely studied in the field of thin film transistors,[1−3] light-emitting diodes,[4] and photovoltaic cells.[5,6] Regioregular poly(3-alkylthiophene)s are particularly promising for use in solar cells due to their relatively high charge mobility derived from their highly crystalline conformation.[7] Among them, poly(3-hexylthiophene) (P3HT) has generally provided good results for such devices.[8] However, its energy band gap and highest occupied molecular orbital (HOMO) level are slightly higher than the best value for solar cell devices.[9] There are a few reports on the synthesis of PTs with introduced aromatic groups at the 3-position that decreases the energy band gaps derived from a longer conjugation length.[10−12] When aromatic groups are directly introduced to the ring at the 3-position of the thiophene, the electron density of the PT $\pi$-conjugation chains and rigidity of its main chains can be changed, and thereby the polymer would have a different optoelectronic property as compared to other poly(3-alkylthiophene)s. Pei et al. first reported the synthesis of poly(3-(4-octylphenyl)thiophene) (POPT) using $FeCl_3$ as an oxidant based on the idea that the introduction of a phenyl ring to the side chain would extend the conjugation length; however, the regioregularity was not considered.[10] Haba et al. then synthesized poly(3-(4-dodecylphenyl)-thiophene) by using vanadium acetylacetonate as an oxidant and achieved a regioregularity of 91%.[11] Dagron-Lartigau et al. also reported the synthesis of a high-molecular-weight and regioregular POPT by Grignard metathesis (GRIM) polymerization.[12] This polymerization system is an efficient synthetic method for regioregular conjugated polymers recently developed by McCullough et al.[13] and further modified by Yokozawa et al.[14] There are two interesting features of the GRIM system. One is to obtain a conjugated polymer with high regioregularity over 95%, and the other is its quasi-living chain growth mechanism,[15] which could lead to a low polydispersity index (PDI) and the possibility of developing block copolymers. However, in Dagron-Latigau's paper, the detailed synthetic conditions and polymer characterization were not included, and the PDI of the polymer was broad.[12]

We now report the synthesis and optoelectronic properties of poly(3-(4′-(3″,7″-dimethyloctoxy)phenyl)thiophene) (P3PhT) and poly(3-(4′-(3″,7″-dimethyloctoxy)-3′-pyridinyl)thiophene) (P3PyT) having a high regioregularity and low PDI. Introducing phenyl and pyridinyl groups at the 3-position of the thiophene rings is expected to decrease the band gaps by extending the conjugation length. In addition, the electron-withdrawing groups lead to lower both of HOMO and lowest unoccupied molecular orbital (LUMO) levels. Thus, this method will be one of the best ways to achieve the maximum potential for polymer solar cells (PSCs). Especially, introducing a pyridinyl group at the 3-position of the thiophene rings has never been reported to the best of our knowledge. These polymers were characterized by proton and carbon nuclear magnetic resonance ($^1$H and $^{13}$C NMR) spectroscopy, size exclusion chromatography (SEC), differential

*To whom correspondence should be addressed: e-mail thigashihara@polymer.titech.ac.jp (T.H.), ree@postech.edu (M.R.), ueda.m.ad@m.titech.ac.jp (M.U.); Tel +81-3-5734-2126 (T.H.), +82-54-279-2120 (M.R.), +81-3-5734-2127 (M.U.); Fax +81-3-5734-2127 (T.H., M.U.), +82-54-279-3399 (M.R.).


Published on Web 01/19/2011

scanning calorimetry (DSC), grazing incidence wide-angle X-ray scattering (GIWAXS), ultraviolet−visible (UV−vis) spectroscopy, fluorescence spectroscopy, and cyclic voltammetry (CV).

## Experimental Section

**Materials.** Tetrahydrofuran (THF) was dried over sodium benzophenone and distilled before use under nitrogen. Thiophene-3-ylboronic acid was prepared according to the literature.[16] Lithium chloride was dried by a heat gun under reduced pressure and used under nitrogen. All other reagents and solvents were used without further purification.

**Synthesis of 3-(4′-(3″,7″-Dimethyloctoxy)phenyl)thiophene (1).** 4-(Thiophene-3-yl)phenol (3.5 g, 19.9 mmol), 1-bromo-3,7-dimethyloctane (11.8 g, 53.4 mmol), $K_2CO_3$ (4.2 g, 30.3 mmol), and acetone (200 mL) were placed in a 500 mL round-bottomed flask under nitrogen, and the reaction mixture was stirred at 75 °C for 12 h. After the reaction, the solvent was evaporated, and the mixture was extracted with ethyl acetate, washed with water, and dried over $MgSO_4$. After filtration, the solvent was removed by evaporation under reduced pressure. The residue was purified by silica gel column chromatography (eluent: hexane) to give 3-(4′-(3″,7″-dimethyloctoxy)phenyl)thiophene as a white solid (1.0 g, 97%); mp =73.8−74.5 °C. $^1$H NMR (300 MHz, $CDCl_3$, ppm, 25 °C): $\delta$ = 7.51 (d, ArH, 2H), 7.35 (m, ArH, 3H), 6.93 (d, ArH, 2H), 4.02 (m, −O−$CH_2$, 2H), 1.90−0.80 (m, alkyl, 19H). $^{13}$C NMR (300 MHz, $CDCl_3$, ppm, 25 °C): $\delta$ = 158.6, 142.2, 128.6, 127.6, 126.3, 126.1, 118.9, 114.8, 66.5, 39.4, 37.4, 36.3, 30.0, 28.1, 24.8, 22.9, 22.8, 19.8. Anal. Calcd for $C_{20}H_{28}OS$; C, 75.90; H, 8.92; O, 5.06; S, 10.13. Found: C, 76.00; H, 8.87.

**Synthesis of 2-Bromo-3-(4′-(3″,7″-dimethyloctoxy)phenyl)thiophene (2).** *N*-Bromosuccinimide (1.68 g, 9.44 mmol) was added to a stirred solution of 3-(4′-(3″,7″-dimethyloctoxy)phenyl)-thiophene (2.98 g, 9.42 mmol) in THF (40 mL) at 0 °C under a nitrogen atmosphere, and the mixture was stirred at room temperature for 12 h. The solvent was evaporated, and hexane was added to the mixture. After stirring for 3 h, succinimide was filtrated and the filtrate was removed by evaporation under reduced pressure. The residue was 2-bromo-3-(4′-(3″,7″-dimethyloctoxy)phenyl)thiophene as a yellow oil (3.68 g, 99%). $^1$H NMR (300 MHz, $CDCl_3$, ppm, 25 °C): $\delta$ = 7.47 (d, ArH, 2H), 7.28 (d, ArH, 1H), 7.00 (d, ArH, 1H), 6.95 (d, ArH, 2H), 4.03 (m, −O−$CH_2$, 2H), 1.91−0.83 (m, Alkyl, 19H). $^{13}$C NMR (300 MHz, $CDCl_3$, ppm, 25 °C): $\delta$ = 158.8, 141.0, 129.9, 129.2, 127.4, 125.8, 114.4, 107.9, 66.4, 39.4, 37.4, 36.3, 30.0, 28.1, 24.8, 22.9, 22.8, 19.8. Anal. Calcd for $C_{20}H_{27}BrOS$; C, 60.75; H, 6.88; Br, 20.21; O, 4.05; S, 8.11. Found: C, 60.88; H, 6.82.

**Synthesis of 2-Bromo-3-(4′-(3″,7″-dimethyloctoxy)phenyl)-5-iodothiophene (3).** To a stirred solution of 2-bromo-3-(4′-(3″,7″-dimethyloctoxy)phenyl)thiophene (1.00 g, 2.52 mmol) in $CHCl_3$ (15 mL) were added iodine (0.35 g, 1.38 mmol) and iodobenzene diacetate (0.49 g, 1.52 mmol) successively at 0 °C under a nitrogen atmosphere, and the mixture was stirred at room temperature for 12 h. Then 10% aqueous $Na_2S_2O_3$ solution was added, and the mixture was extracted with $CHCl_3$. The organic layer was washed with water and dried over anhydrous $MgSO_4$. After filtration, the solvent was removed by evaporation under reduced pressure. The residue was purified by silica gel column chromatography (eluent: hexane) to give 2-bromo-3-(4′-(3″,7″-dimethyloctoxy)phenyl)-5-iodothiophene as a yellow oil (1.11 g, 85%). $^1$H NMR (300 MHz, $CDCl_3$, ppm, 25 °C): $\delta$ = 7.42 (d, ArH, 2H), 7.17 (s, ArH, 1H), 6.95 (d, ArH, 2H), 4.03 (m, −O−$CH_2$, 2H), 1.92−0.86 (m, Alkyl, 19H). $^{13}$C NMR (300 MHz, $CDCl_3$, ppm, 25 °C): $\delta$ = 159.1, 143.1, 138.7, 129.8, 126.0, 114.5, 110.7, 72.0, 66.5, 39.4, 37.4, 36.3, 30.0, 28.1, 24.8, 22.9, 22.8, 19.8. Anal. Calcd for $C_{20}H_{26}BrIOS$; C, 46.08; H, 5.03; Br, 15.33; I, 24.34; O, 3.07; S, 9.15. Found: C, 46.11; H, 4.83.

**Synthesis of 5-Bromo-2-(3′,7′-dimethyloctyloxy)pyridine (4).** 3,7-Dimethyl-1-octanol (8.0 mL, 41.9 mmol) was dropped in a solution of NaH (2.81 g, 70.2 mmol) in THF (60 mL) at room temperature with a stream of nitrogen. The reaction mixture was stirred for 1 h; a solution of 5-bromo-2-iodopyridine (10.0 g, 35.2 mmol) in THF (20 mL) and CuBr (cat.) were added. The reaction mixture was refluxed for 18 h and cooled to room temperature. The solvent was evaporated, and the mixture was extracted with $CHCl_3$. The organic layer was washed with water and dried over anhydrous $MgSO_4$. After the drying agent was removed by filtration, the solvent was removed by evaporation under reduced pressure. The residue was purified by silica gel column chromatography (eluent: $CH_2Cl_2$ and hexane) to give 5-bromo-2-(3′,7′-dimethyloctyloxy)pyridine as a clear oil (8.3 g, 75%). $^1$H NMR (300 MHz, $CDCl_3$, ppm, 25 °C): $\delta$ = 8.17 (d, ArH, 1H), 7.61 (q, ArH, 1H), 6.62 (d, ArH, 1H), 4.27 (m, −O−$CH_2$, 2H), 1.87−0.77 (m, alkyl, 19H). $^{13}$C NMR (300 MHz, $CDCl_3$, ppm, 25 °C): $\delta$ = 163.0, 147.6, 141.1, 112.9, 111.5, 65.0, 39.4, 37.4, 36.0, 30.0, 28.1, 24.8, 22.9, 22.8, 19.8. Anal. Calcd for $C_{15}H_{24}BrNO$; C, 57.33; H, 7.70; Br, 25.43; N, 4.46; O, 5.09. Found: C, 57.32; H, 7.52; N, 4.42.

**Synthesis of 3-(4′-(3″,7″-Dimethyloctoxy)-3′-pyridinyl)thiophene (5).** 5-Bromo-2-(3′,7′-dimethyloctyloxy)pyridine (1.0 g, 3.18 mmol), thiophene-3-ylboronic acid (0.82 g, 6.36 mmol), $K_2CO_3$ (3 g, 22 mmol), Aliquat 336 (cat.), toluene (20 mL), THF (10 mL), and $H_2O$ (5 mL) were placed in a 100 mL round-bottomed flask. The mixture was stirred and degassed, and then $Pd(PPh_3)_4$ (0.1 g, 0.09 mmol) was added. The mixture was refluxed for 24 h and cooled to room temperature. The solvent was evaporated, and the mixture was extracted with ethyl acetate. The organic layer was washed with brine and dried over anhydrous $MgSO_4$. After the drying agent was removed by filtration, the solvent was removed by evaporation under reduced pressure. The residue was purified by silica gel column chromatography (eluent: hexane and $CH_2Cl_2$) to give 3-(4′-(3″,7″-dimethyloctoxy)-3′-pyridinyl)thiophene as a clear oil (1.0 g, 97%). $^1$H NMR (300 MHz, $CDCl_3$, ppm, 25 °C): $\delta$ = 8.40 (d, ArH, 1H), 7.77 (q, ArH, 1H), 7.42−7.31 (m, ArH, 3H), 6.76 (d, ArH, 1H), 4.34 (m, −O−$CH_2$, 2H), 1.89−0.82 (m, Alkyl, 19H). $^{13}$C NMR (300 MHz, $CDCl_3$, ppm, 25 °C): $\delta$ = 163.4, 144.6, 139.2, 136.9, 126.7, 126.0, 125.2, 119.7, 111.1, 64.8, 39.4, 37.5, 36.2, 30.1, 28.1, 24.8, 22.9, 22.8, 19.9. Anal. Calcd for $C_{19}H_{27}NOS$; C, 71.88; H, 8.57; N, 4.41; O, 5.04; S, 10.10. Found: C, 72.63; H, 8.74; N, 4.23.

**Synthesis of 2-Bromo-3-(4′-(3″,7″-dimethyloctoxy)-3′-pyridinyl)thiophene (6).** *N*-Bromosuccinimide (0.56 g, 3.15 mmol) was added to a stirred solution of 3-(4′-(3″,7″-dimethyloctoxy)-3′-pyridinyl)thiophene (1.0 g, 3.15 mmol) in THF (10 mL) at 0 °C under a nitrogen atmosphere, and the mixture was stirred at room temperature for 2.5 h. The solvent was evaporated, and hexane was added to the mixture. After stirring for 1 h, succinimide was filtrated and the filtrate was removed by evaporation under reduced pressure. The residue, 2-bromo-3-(4′-(3″,7″-dimethyloctoxy)-3′-pyridinyl)thiophene, was obtained as a clear oil (1.2 g, 95%). $^1$H NMR (300 MHz, $CDCl_3$, ppm, 25 °C): $\delta$ = 8.34 (d, ArH, 1H), 7.77 (q, ArH, 1H), 7.32 (d, ArH, 1H), 7.00 (d, ArH, 1H), 6.78 (d, ArH, 1H), 4.36 (m, −O−$CH_2$, 2H), 1.89−0.83 (m, alkyl, 19H). $^{13}$C NMR (300 MHz, $CDCl_3$, ppm, 25 °C): $\delta$ = 163.4, 146.6, 138.7, 138.0, 128.7, 126.3, 124.0, 110.7, 108.9, 64.7, 39.4, 37.4, 36.1, 30.0, 28.1, 24.8, 22.9, 22.8, 19.8. Anal. Calcd for $C_{19}H_{26}BrNOS$; C, 57.57; H, 6.61; Br, 20.16; N, 3.53; O, 4.04; S, 8.09. Found: C, 57.94; H, 6.58; N, 3.52.

**Synthesis of 2-Bromo-3-(4′-(3″,7″-dimethyloctoxy)-3′-pyridinyl)-5-iodothiophene (7).** To a stirred solution of 2-bromo-3-(4′-(3″,7″-dimethyloctoxy)-3′-pyridinyl)thiophene (0.94 g, 2.37 mmol) in $CHCl_3$ (5 mL) at room temperature were added iodine (0.352 g, 1.39 mmol) and iodobenzene diacetate (0.487 g, 1.51 mmol) successively, and the mixture was stirred for 3 days. Then 10% aqueous $Na_2S_2O_3$ solution was added, and the mixture was extracted with $CHCl_3$. The organic layer was washed with brine and water and dried over anhydrous $MgSO_4$. After the drying agent was removed by filtration, the solvent was removed by

evaporation under reduced pressure. The residue was purified by silica gel column chromatography (eluent: hexane and $CH_2Cl_2$) to give 2-bromo-3-(4′-(3″,7″-dimethyloctoxy)-3′-pyridinyl)-5-iodothiophene as a pale yellow oil (1.05 g, 85%). $^1$H NMR (300 MHz, $CDCl_3$, ppm, 25 °C): $\delta$ = 8.29 (d, ArH, 1H), 7.70 (q, ArH, 1H), 7.15 (s, ArH, 1H), 6.77 (d, ArH, 1H), 4.35 (m, $-O-CH_2$, 2H), 1.88−0.82 (m, Alkyl, 19H). $^{13}$C NMR (300 MHz, $CDCl_3$, ppm, 25 °C): $\delta$ = 163.7, 146.6, 140.2, 138.6, 138.2, 122.8, 111.8, 110.9, 64.9, 39.4, 37.4, 36.1, 30.1, 28.1, 24.8, 22.9, 22.8, 19.8. Anal. Calcd for $C_{19}H_{25}BrINOS$; C, 43.69; H, 4.82; Br, 15.30; I, 24.30; N, 2.68; O, 3.06; S, 6.14. Found: C, 43.75; H, 4.68; N, 2.66.

**Synthesis of Poly(3-(4′-(3″,7″-dimethyloctoxy)phenyl)thiophene) (P3PhT).** A round-bottomed flask equipped with a three-way stopcock was charged with lithium chloride (0.10 g, 2.36 mmol) and was heated by a heat gun under reduced pressure. After the flask was cooled to room temperature under a nitrogen atmosphere, compound **3** (346 mg, 0.663 mmol) and THF (25 mL) were added, and the mixture was stirred at 0 °C for 30 min. To the mixture was added isopropylmagnesium chloride ($^i$PrMgCl) (2.0 M solution in THF, 0.364 mL, 0.729 mmol) via a syringe, and the mixture was stirred for 30 min. Then, a suspension of [1,3-bis(diphenylphosphino)propane]nickel(II) dichloride (Ni(dppp)$Cl_2$) (10.0 mg, 0.0185 mmol) in dry THF (5.0 mL) was added to the mixture via a syringe, and then the mixture was stirred at room temperature for 7 h. The polymerization was quenched by the addition of 5 M HCl solution. The polymer solution was poured into a mixture solution of methanol (200 mL) and water (200 mL), and the residue was filtered and dried under reduced pressure to give P3PhT ($\overline{M_n}$ = 8900, PDI = 1.05) as a purple solid (0.145 g, 70%). $T_m$ = 258 °C. $^1$H NMR (300 MHz, $CDCl_3$, ppm, 25 °C): $\delta$ = 7.26 (d, ArH, 2H), 6.88 (d, ArH, 2H), 6.82 (s, ArH, 1H), 4.00 (t, $-OCH_2$, 2H), 1.90−0.83 (m, alkyl, 19H). Anal. Calcd C, 76.43; H, 8.28; O, 5.10; S, 10.19. Found: C, 74.92; H, 8.17.

**Synthesis of Poly(3-(4′-(3″,7″-dimethyloctoxy)-3′-pyridinyl)-thiophene) (P3PyT).** A round-bottomed flask equipped with a three-way stopcock was charged with lithium chloride (0.21 g, 4.95 mmol) and was heated by a heat gun under reduced pressure. After the flask was cooled to room temperature under a nitrogen atmosphere, compound **7** (501 mg, 0.960 mmol) and THF (20 mL) were added, and the mixture was stirred at 0 °C for 30 min. To the mixture was added $^i$PrMgCl (2.0 M solution in THF, 0.528 mL, 1.05 mmol) via a syringe, and the mixture was stirred for 30 min. Then, a suspension of Ni(dppp)$Cl_2$ (10.0 mg, 0.0185 mmol) in dry THF (5.0 mL) was added to the mixture via a syringe, and then the mixture was stirred at 40 °C for 24 h. The polymerization was quenched by the addition of 5 M HCl solution. The polymer solution was poured into a mixture solution of methanol (200 mL) and water (200 mL), and the residue was filtered and washed by Soxhlet extraction using methanol and acetone and finally extracted using $CHCl_3$. The solvent was removed by evaporation under reduced pressure to give P3PyT ($\overline{M_n}$ = 27 000, PDI = 1.19) as a purple solid (0.229 g, 76%). $T_g$ = 20 °C. $^1$H NMR (300 MHz, $CDCl_3$, ppm, 25 °C): $\delta$ = 8.14 (d, ArH, 1H), 7.55 (m, ArH, 1H), 6.85 (s, ArH, 1H), 6.72 (d, ArH, 1H), 4.32 (t, $-OCH_2$, 2H), 1.89−0.81 (m, alkyl, 19H). Anal. Calcd: C, 71.26; H, 8.43; Br, 0.89; N, 4.37; O, 5.00; S, 10.03. Found: C, 71.88; H, 7.95; N, 4.31.

**Measurements.** The $^1$H and $^{13}$C NMR spectra were recorded with a Bruker DPX300S spectrometer. Number- and weight-average molecular weights ($M_n$ and $M_w$) were measured by SEC on a Jasco GULLIVER 1500 system equipped with two polystyrene gel columns (Plgel 5 $\mu$m MIXED-C) eluted with $CHCl_3$ at a flow rate of 1.0 mL min$^{-1}$ calibrated by standard polystyrene samples. Thermal analysis was performed on a Seiko EXSTAR 6000 TG/DTA 6300 thermal analyzer at a heating rate of 10 °C/min for thermogravimetry (TG) and DSC 6200 at a heating rate of 20 °C/min for DSC under nitrogen. UV−vis spectra of polymer thin films and solution in $CHCl_3$ at $10^{-5}$ mol/L were taken on a Jasco V-560 UV/vis spectrophotometer over a wavelength range of 300−800 nm. Fluorescence spectra of polymer solution in $CHCl_3$ at $5 \times 10^{-6}$ mol/L were taken on a Jasco FP-750 spectrofluorometer over a wavelength range of 500−700 nm. CV measurements were performed at room temperature using a working electrode (ITO, polymer film area of about 10 × 20 mm$^2$), a reference electrode (Ag/AgCl), and a counter electrode (Pt wire) at a sweep rate of 0.1 V/s (HSV-100 Hokuto Denko). A 0.1 M solution of tetrabutylammonium perchlorate in anhydrous acetonitrile was used as an electrolyte. The energy level of HOMO was determined from the onset oxidation ($E_{onset}^{OX}$) based on the reference energy level of ferrocene (4.8 V below the vacuum level) according to the following equation: HOMO = $-e(E_{onset}^{OX} - E_{ferrocene}^{1/2} + 4.8)$ (eV). The LUMO level was calculated from the HOMO and the value of optical band gap according to the equation LUMO = HOMO + energy band gap (eV).

GIWAXS measurements were conducted at the 4C1 and 4C2 beamlines[17,18] of the Pohang Accelerator Laboratory at Pohang University of Science & Technology.[19] The film samples (which were coated with 50−70 nm thickness on silicon (Si) substrates) were mounted on a homemade $z$-axis goniometer equipped in a vacuum chamber. The incident angle $\alpha_i$ of the X-ray beam was set at 0.16°, which is between the critical angles of the films and the Si substrate ($\alpha_{c,f}$ and $\alpha_{c,s}$). Scattering data were measured at a sample-to-detector distance of 120.4 mm using an X-ray radiation source of 0.138 nm wavelength and a two-dimensional (2D) charge-coupled detectors (CCD) (Mar USA). All scattering measurements were carried out at 25 °C. Each measurement was collected for 30 s.

## Results and Discussion

**Synthesis of Monomers.** To prepare PTs with low-energy band gaps and HOMO levels, we selected two kinds of thiophene monomers containing phenyl and pyridinyl groups. These thiophene units have an electron density lower than that of P3HT due to the electron-withdrawing pyridinyl and phenyl groups. We expect that these PTs have lower energy band gaps due to the extended aromatic conjugation by the side chain and lower HOMO levels due to low electron density than those of P3HT. Furthermore, a 3,7-dimethyloctoxy group was introduced to increase the solubility of the PTs. The key steps in the monomer synthesis are bromination and iodination at the 2- and 5-positions of the 3-aromaticthiopenes, respectively. This enables the selective synthesis of a product with magnesium halide at the 5-position, which leads to the regioregular PTs. These two monomers were successfully prepared in three steps (Scheme 1) and four steps (Scheme 2) and then identified by $^1$H NMR (Figures S1 and S3) and $^{13}$C NMR (Figures S2 and S4) spectra, respectively.

**Synthesis of Polymers.** We first examined the Grignard exchange reaction of the monomers **3** and **7** with an equivalent of $^i$PrMgCl in the presence of LiCl in THF at 0 °C for 30 min, followed by quenching with methanol under the same conditions reported in a previous study.[20] The quantitative Grignard exchange reaction at 5-position was confirmed by the $^1$H NMR spectra of each resulting product.

On the basis of these results, the nickel-catalyzed coupling polymerizations of compounds **3** and **7** were carried out at room temperature in THF in the presence of LiCl (Scheme 3). The polymerization of compound **3** successfully proceeded to give P3PhT with a very low PDI (Table 1). On the other hand, both the $\overline{M_n}$ and yield of P3PyT by the polymerization of **7** were low. Thus, to improve the $\overline{M_n}$ and yield, the polymerization was carried out at 40 °C to produce P3PyT with the high $\overline{M_n}$ of 27 000 g/mol in 76% yield. The structures of P3PhT and P3PyT were characterized by $^1$H NMR and SEC

**Scheme 1. Synthesis of Compound 3**

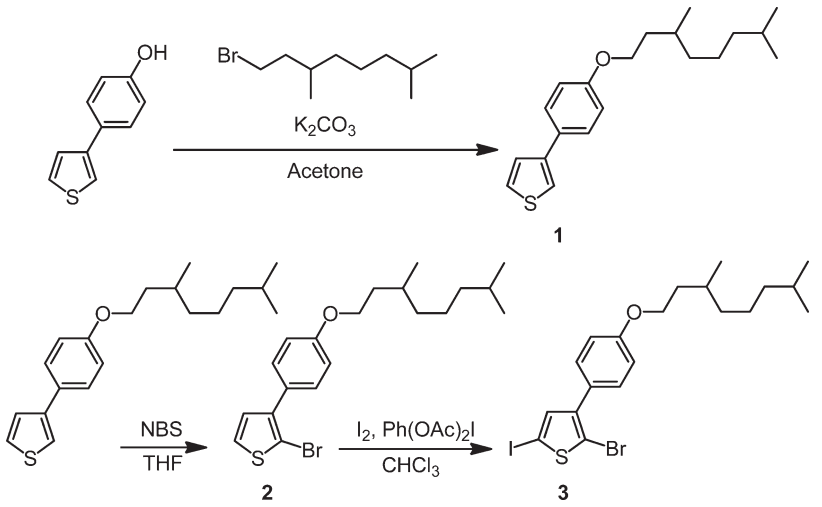


**Scheme 2. Synthesis of Compound 7**

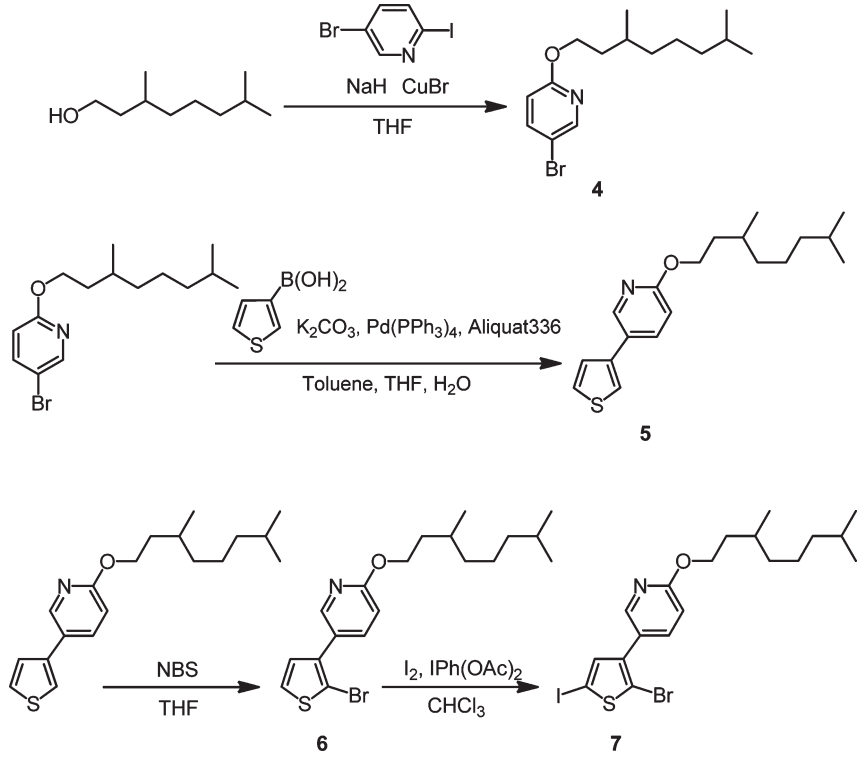


**Scheme 3. Synthesis of P3PhT and P3PyT**

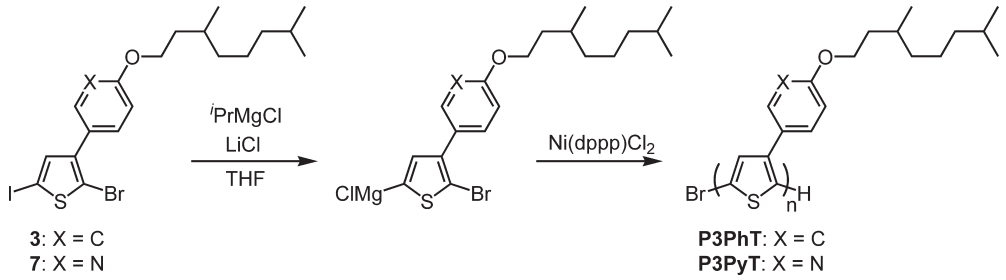


profiles. Figures 1 and 2 show the $^1$H NMR spectra of P3PhT and P3PyT, in which the characteristic signals assignable to the oxymethylene protons appear at 4.00 and 4.32 ppm, respectively. P3PhT and P3PyT have very high regioregularities of 95% and 99%, respectively, estimated by comparing the signal intensities of the protons at the 4-positions of the thiophene ring with head-to-tail (6.82 ppm in P3PhT and 6.85 ppm in P3PyT) and tail-to-tail (6.96 ppm in

P3PhT and 7.05 ppm in P3PyT) structures.[11] Figure 3 shows the SEC profiles of P3PhT and P3PyT, which displayed almost unimodal peaks with a low PDI. The small shoulder peaks may be due to the polymer/polymer coupling reactions.

**Thermal Properties.** The thermal properties of P3PhT and P3PyT were evaluated by TGA (Figure S5) and DSC (Figure 4), respectively. P3PhT exhibited a relatively high degradation temperature (5% weight loss) of 390 °C under nitrogen, while its melting point ($T_m$) was observed at 258 °C and no glass transition temperature ($T_g$) was observed. This indicates that P3PhT is a crystalline polymer, probably due to the high $\pi$-stacking of the 3-phenylthiopene units. P3PyT also exhibited a degradation temperature (5% weight loss) of 360 °C under nitrogen and showed an amorphous nature with a $T_g$ (= 20 °C) and no $T_m$. As compared to P3PhT, P3PyT shows an amorphous nature contrary to our expectation, probably because P3PyT has a very weak $\pi$-stacking derived from the poor electron density of the pyridinyl linker as well as less coplanarity of the pyridinyl linker to the thiophene backbone unit.

**Table 1. Synthesis of Homopolythiophenes**[a]

| sample | temp (°C) | time (h) | $\overline{M_n}^b$ | PDI[b] | yield (%) |
|---|---|---|---|---|---|
| P3PhT | r.t. | 7 | 8900 | 1.05 | 70 |
| P3PyT | 40 | 24 | 27000 | 1.19 | 76 |

[a] [LiCl]/[M] = 5 THF = 25 mL. [*i*-PrMgCl]/[M] = 1.0. [b] Determined by SEC ($CHCl_3$, PSt standard).

**Structural Characteristics.** Parts a and b of Figure 5 show the representative 2D GIWAXS patterns of the P3PhT and P3PyT thin films coated on Si substrates, respectively. From these 2D scattering patterns, the out-of-plane and in-plane scattering profiles have been extracted along the $\alpha_f$ direction at $2\theta_f = 0°$ and along the $2\theta_f$ direction at $\alpha_f = 0.16°$, respectively, and displayed in Figure 6.

As can be seen in Figure 6a, the out-of-plane profile of P3PhT clearly reveals four scattering spots, and their relative scattering vector lengths from the specular reflection position are 1, 2, 3, and 5. These scattering spots are not detected in the in-plane profile (Figures 5a and 6b). Therefore, the appearance of these high order scattering spots strongly indicates that a well-ordered multilayer structure (lamellar structure) is formed in the film, and its layers are stacked along a direction normal to the film plane. The first-order peak appears at $\alpha_f = 2.57°$ and $2\theta_f = 0°$, giving a *d*-spacing of 3.08 nm. This *d*-spacing value corresponds to the long period in the lamellar structure. This long period is close to, but not smaller than, twice the length (1.52 nm) of the fully extended bristle; here the length of the bristle in the fully extended conformation was estimated by performing a molecular simulation with the Cerius[2] software package (Accelrys,

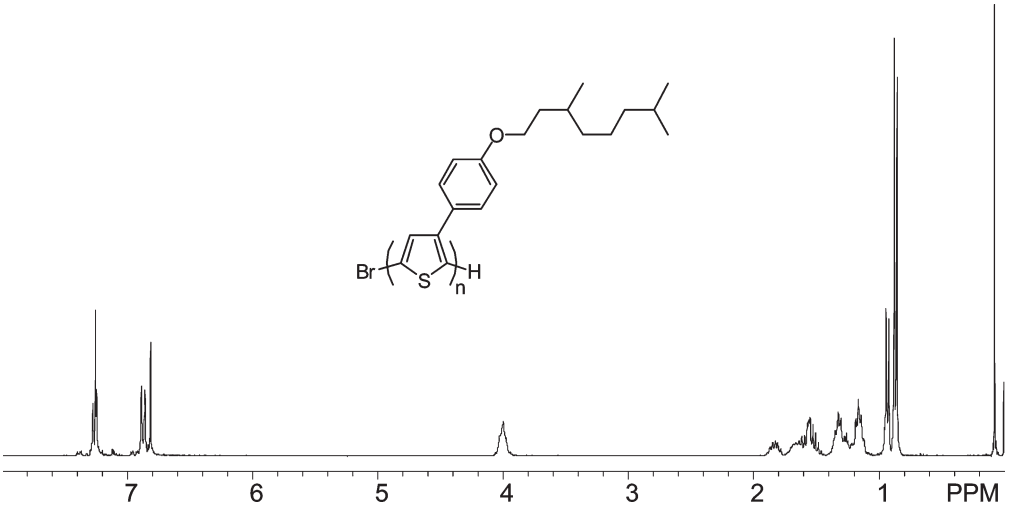


**Figure 1.** $^1H$ NMR spectrum of P3PhT in $CDCl_3$.

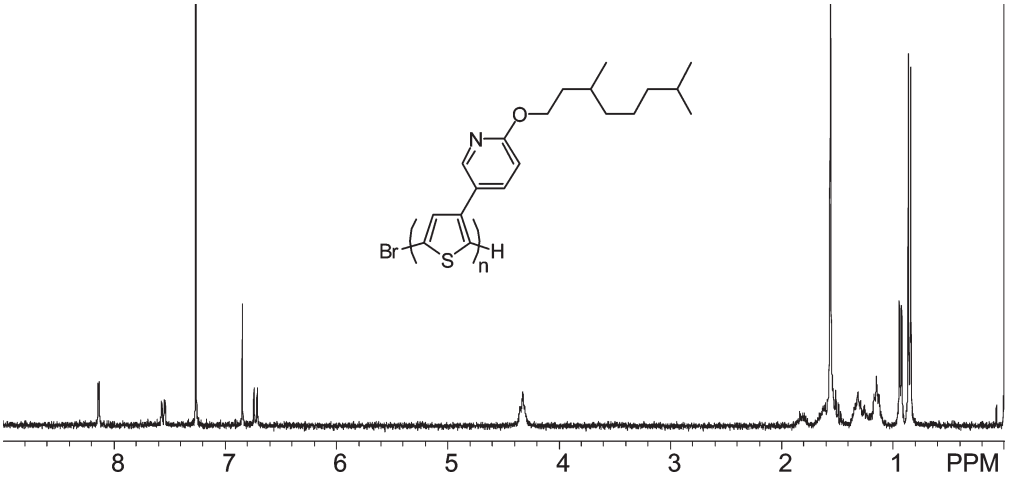


**Figure 2.** $^1H$ NMR spectrum of P3PyT in $CDCl_3$.

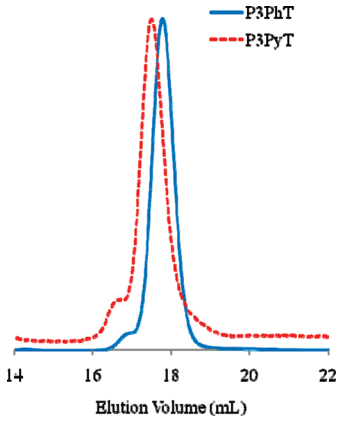


**Figure 3.** SEC profiles of P3PhT and P3PyT.

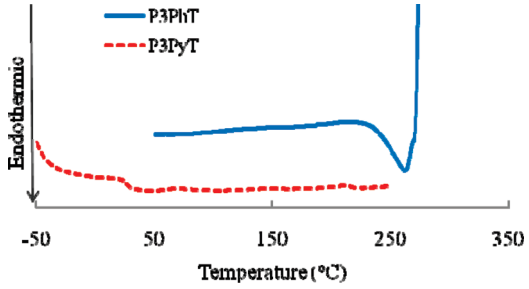


**Figure 4.** DSC profiles of P3PhT and P3PyT.

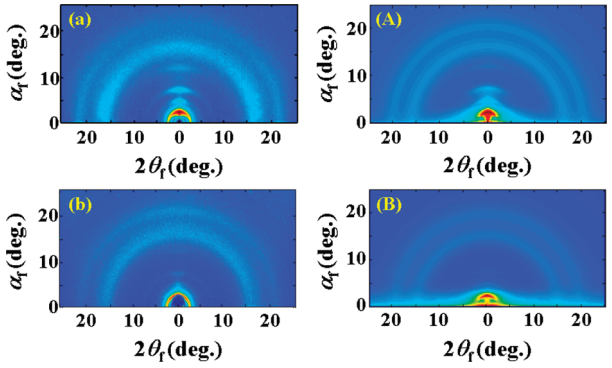


**Figure 5.** 2D GIWAXS patterns measured at $\alpha_i = 0.16°$ for (a) P3PhT and (b) P3PyT in thin films casted on silicon substrates; the measurements were conducted at 25 °C. 2D GIWAXS patterns simulated for (A) P3PhT and (B) P3PyT from the determined structural parameters (Table 2) using the GIXS formula.

San Diego, CA). This fact indicates that there is no interdigitation between the bristles of the adjacent molecular layers.

On the other hand, the in-plane scattering profile of P3PhT shows two broad peaks at $2\theta_f = 15.73°$ and 20.18° (Figure 6b). In the 2D scattering pattern, the broad peak at $2\theta_f = 15.73°$ is isotropic in the 2D scattering pattern (Figure 5a), whereas the peak at $2\theta_f = 20.18°$ is somewhat anisotropic rather than isotropic. As discussed earlier, the DSC analysis found that P3PhT has a crystalline nature whose $T_m$ is around 258 °C. One may expect that the aliphatic bristle parts in P3PhT are associated with a crystal formation. However, the observed $T_m$ is unusually too high for the melting point expected for the aliphatic bristle parts in a crystalline phase. Furthermore, the aliphatic bristle part has two branching points which can have a negative effect on the crystal formation. Therefore, the observed high $T_m$ is attributed to the melting of the

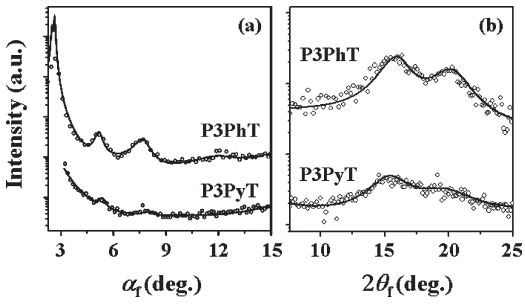


**Figure 6.** (a) Out-of-plane scattering profiles extracted from the 2D GIWAXS patterns (Figure 5a,b) along the $\alpha_f$ direction at $2\theta_f = 0°$. (b) In-plane scattering profiles extracted from the 2D GIWAXS patterns (Figure 5a,b) along the $2\theta_f$ direction at $\alpha_f = 0.16°$. The symbols represent the measured data, and the solid lines were obtained by fitting the data with the GIXS formula.

ordered thiophene backbone chains with or without the 3-positioned phenyl linker. As can be seen in Figure 5a, the P3PhT film, however, shows no diffraction signals from any regular crystal lattice structure, suggesting that the thiophene backbone chains with or without the 3-positioned phenyl linker are in an ordered phase without any regular crystal lattice. Taking these results into account, the first broad peak at $2\theta_f = 15.73°$, which has a *d*-spacing of 0.50 nm ($= d_{r1}$), can be assigned to an amorphous halo diffraction from the mean distance between the noncrystalline aliphatic bristles. The second one at $2\theta_f = 20.18°$, which was determined to have a *d*-spacing of 0.39 nm ($= d_{r2}$), is attributed to the mean distance between the interchain stacks of the thiophene backbones with or without the 3-positioned phenyl linker.

On the basis of this qualitative structural information, a lamellar structure is proposed as shown in Figure 7a. With this structural model, we attempted to quantitatively analyze the scattering data using a GIXS formula,[21,22] which was derived using the distorted wave Born approximation. As can be seen in Figure 6, the out-of-plane and in-plane scattering profiles of P3PhT can be satisfactorily fitted using the GIXS formula combined with the multilayered structure model. The data analysis results are summarized in Table 2. Moreover, the electron density profile along the film thickness direction has been determined and displayed in Figure 7a. It is noted that the mean orientation angle $\varphi$ of the lamellar structure with respect to the out-of-plane projection is 0.0°, but its deviation $\sigma_\varphi$ is 9.3°, which is not small enough. In the lamellar structure, the long period ($d_3$) is 3.08. Each lamella is composed of two sublayers, namely ordered and amorphous layers. The ordered (i.e., crystalline) and amorphous sublayers have a thickness of 1.43 nm ($= l$) and 1.65 nm ($= d_3 - l$), respectively. The amorphous sublayer is composed of a bilayer formed from the aliphatic bristles with no interdigitation. The crystalline sublayer thickness is equivalent to the diameter of the thiophene backbone with the 3-positioned phenyl linker (i.e., 3-phenylthiophene backbone). Therefore, the result confirms that the crystalline sublayer consists of thiophene and a 3-positioned phenyl linker. This result indicates that the thiophene backbone unit and phenyl linker are more likely coplanar, therefore enhancing the $\pi$–$\pi$ interaction between the polymer backbone chains and resulting in the longer $\pi$-conjugation length of P3PhT. From the characteristics of the crystalline sublayer, its corresponding scattering peak ($2\theta_f = 20.18°$) is expected to anisotropically appear. However, as discussed above, its anisotropy is weak (Figure 5a). This result might be attributed to the following possible three factors: the relatively high deviation of the mean orientation

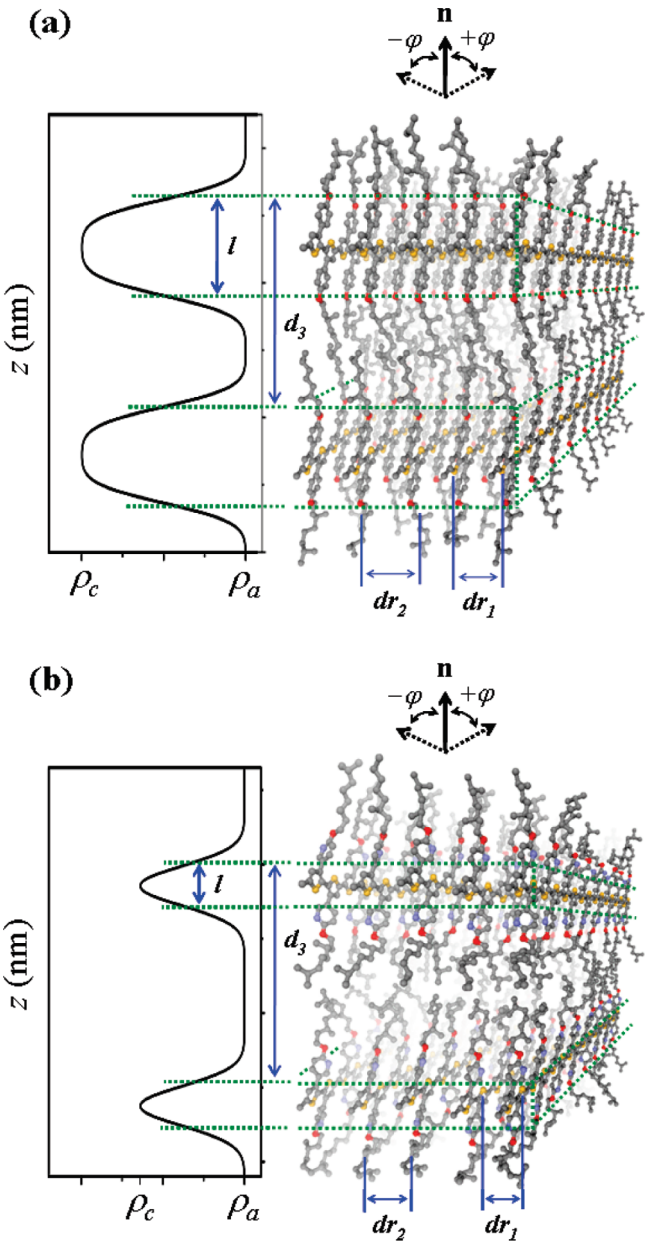


**Figure 7.** Molecular model of a multilayer structure (i.e., lamellar structure) formed in (a) P3PhT and (b) P3PyT films on silicon substrates. Each lamella consists of two sublayers, namely an ordered layer and an amorphous layer: $d_3$ is the long period of the lamellar stack; $l$ is the thickness of the ordered sublayer in a lamella; $d_{r1}$ is the mean interdistance of bristles in the amorphous sublayer; $d_{r2}$ is the mean interdistance of polymer backbone chains. For P3PhT, the ordered sublayer consists of laterally stacked 3-phenylthiophene backbone chains while the amorphous sublayer is composed of a bilayer formed from the aliphatic bristles with no interdigitation. For P3PyT, the ordered sublayer consists of laterally stacked thiophene backbone chains while the amorphous sublayer is composed of a bilayer formed mainly from the pyridinyl-containing aliphatic bristles with no interdigitation. Relative electron density $\rho$ profiles along the $z$-axis (i.e., the direction of the film thickness) in the P3PhT and P3PyT films supported on silicon substrates.

angle, the poor lateral packing order of the 3-phenylthiophene backbones, and the relatively poor long range of the interchain stacking of the 3-phenylthiophene backbones.

From the structural parameters determined above, we attempted to calculate the 2D GIWAXS patterns using the GIXS formula. The calculated 2D scattering pattern compared well with the measured scattering data (Figures 5a and 5A).

**Table 2. Structural Parameters of the P3PhT and P3PyT Thin Film Which Were Determined by GIWAXS Measurements and Data Analysis**

| sample | $d_3$[a] (nm) | $d_{r1}$[b] (nm) | $d_{r2}$[c] (nm) | $l$[d] (nm) | $\sigma_l$[e] | $\bar{\varphi}$[f] (deg) | $\sigma_\varphi$[g] (deg) |
|---|---|---|---|---|---|---|---|
| P3PhT | 3.08 | 0.50 | 0.39 | 1.43 | 0.23 | 0.0 | 9.3 |
| P3PyT | 2.96 | 0.51 | 0.4 | 0.42 | 0.23 | 0.0 | 9.8 |

[a] Long period of multilayer structure (i.e., lamellar structure). [b] Mean interdistance between the aliphatic bristles in the amorphous sublayer. [c] Mean interdistance of the lateral stacks of polymer backbone chains in the ordered sublayer. [d] Mean thickness of the ordered sublayer. [e] Standard deviation of the mean thickness of ordered sublayer. [f] Orientation angle. [g] Standard deviation for orientation angle.

In case of P3PyT, the out-of-plane profile shows relatively weak diffraction peaks compared to the P3PhT film (Figures 5b and 6a). One scattering spot appears at $\alpha_f = 5.35°$ and $2\theta_f = 0°$, and another spot is discernible at $\alpha_f = 8.01°$ and $2\theta_f = 0°$. The $d$-spacing of the scattering spot at $\alpha_f = 5.35°$ and $2\theta_f = 0°$ is determined to be 1.48 nm. This $d$-spacing value is close to the length (1.52 nm) of the fully extended bristle. Another scattering spot at $\alpha_f = 8.01°$ and $2\theta_f = 0°$ is estimated to have a $d$-spacing of 1.00 nm. This $d$-spacing value is almost 2/3 of that of the scattering peak at $\alpha_f = 5.35°$ and $2\theta_f = 0°$. These two peaks are not observed in the in-plane scattering profile (Figures 5b and 6b). Therefore, the two peaks are the second- and third-order reflections of the lamellar structure whose layers stack normal to the film plane. P3PyT also reveals two broad halo peaks as observed for P3PhT (Figures 5a, 5b, and 6b). The halo peaks at $2\theta_f = 15.50°$ and 19.90° are determined to have a $d$-spacing of 0.51 and 0.40 nm, respectively. The 2D scattering pattern is apparently similar to that of P3PhT, but the overall scattering intensity is relatively weaker than that of P3PhT.

Taking into account the DSC result discussed earlier, the above scattering results collectively indicate the following. First, P3PyT also forms a multilayer structure whose layer stacking direction is normal to the film plane. However, P3PyT has a relatively weak self-assembly force in comparison to P3PhT. Second, from the second- and third-order reflections of the lamellar structure, the long period of the lamellar structure is estimated to be 2.96 nm ($= d_3$). This long period is close to, but slightly smaller than, twice the length of the fully extended bristle. Taking into account the amorphous nature of the aliphatic bristles, the determined long period indicates that there is present no interdigitation between the bristles of the adjacent molecular layers. Finally, one halo ring at $2\theta_f = 15.50°$ is attributed to the amorphous characteristic of the bristles, whereas another halo ring is associated with the polymer backbone chains.

On the basis of this qualitative structural information, a multilayer structural model is also proposed for P3PyT (Figure 7b). With this structural model, we attempted to quantitatively analyze the scattering data using a GIXS formula as conducted for P3PhT. The out-of-plane and in-plane scattering profiles of P3PyT were found to be well fitted using the GIXS formula combined with the multilayered structure model (Figure 6). Furthermore, the electron density profile along the film thickness direction was determined (Figure 7b). The obtained structural parameters are listed in Table 2. The mean orientation angle $\bar{\varphi}$ of the lamellar structure with respect to the out-of-plane projection is 0.0°, but its deviation $\sigma_\varphi$ is 9.8°, which is slightly larger than that of P3PhT. The individual lamellae are composed of ordered and amorphous sublayers. The ordered and amorphous sublayers have a thickness of 0.42 nm ($= l$) and 2.54 nm ($= d_3 - l$), respectively. The amorphous sublayer is composed of a bilayer formed from the aliphatic bristles with no

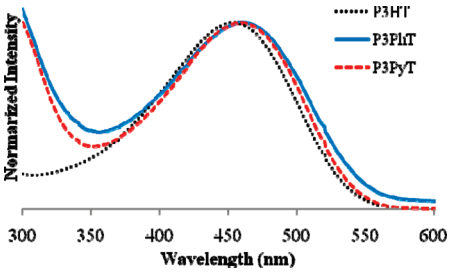


**Figure 8.** UV−vis spectra of P3HT, P3PhT, and P3PyT in $CHCl_3$.

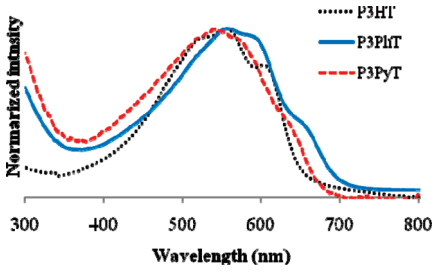


**Figure 9.** UV−vis spectra of P3HT, P3PhT, and P3PyT in films.

interdigitation. The ordered sublayer thickness is equivalent to the diameter of the thiophene backbone itself without the 3-positioned pyridinyl linker, confirming that the ordered sublayer consists of thiophene backbones. This result indicates that the thiophene backbone unit and pyridinyl linker are unlikely coplanar, causing a poor $\pi-\pi$ interaction between the polymer backbone chains, thus resulting in shortening of the $\pi$-conjugation length, compared with P3PhT. Taking these results into account, the halo ring at $2\theta_f = 19.90°$ can be assigned to the reflection for the mean interdistance of the polymer backbone chains ($d_{r2}$). As a result, the halo ring at $2\theta_f = 15.50°$ can further be assigned to the reflection for the mean interdistance of the bristles ($d_{r1}$) in the amorphous phase. It is additionally noted that the isotropic characteristic of the diffraction at $2\theta_f = 19.90°$ might result from several factors, such as a relatively large orientation angle deviation, poor interstacking of the thiophene backbone units, and very thin thickness of the ordered sublayer. From the determined structural parameters in Table 2, a 2D scattering pattern has also been attempted using the GIXS formula. As can be seen in Figures 5b and 5B, the simulated scattering pattern is in good agreement with the measured scattering data.

In comparison, both P3PhT and P3PyT in the thin films reveal a lamellar structure whose layers stack normal to the film plane. For both polymers, the aliphatic bristles always form an amorphous sublayer; however, the phenyl linker in P3PhT is excluded from the amorphous layer because of its coplanarity with the thiophene backbone unit, whereas the pyridinyl linker is included in the amorphous sublayer because of its less coplanarity from the thiophene backbone unit. For the ordered sublayer, its degree of order and thickness are relatively higher and larger in P3PhT, respectively, compared to P3PyT. As a result, P3PhT reveals a relatively longer $\pi$-conjugation length along the polymer backbone when compared to P3PyT.

**Optical and Electronic Properties.** The optical properties of P3HT, P3PhT, and P3PyT were investigated by UV−vis and fluorescence spectroscopies. The solution-state UV−vis spectra of P3HT, P3PhT, and P3PyT show a maximum absorption ($\lambda_{max}$) for the $\pi-\pi^*$ transition at 453, 458, and 461 nm, respectively (Figure 8). Both P3PhT and P3PyT reveal slightly longer $\lambda_{max}$ values than P3HT, indicating that their $\pi$-conjugation lengths are longer than that of P3HT. The high molar absorption coefficients were found to be $\varepsilon_{458} = 1.9 \times 10^5\ M^{-1}\ cm^{-1}$ for P3PhT and $\varepsilon_{461} = 3.3 \times 10^5\ M^{-1}\ cm^{-1}$ for P3PyT, respectively. Furthermore, both P3PhT and P3PyT in chloroform exhibit a bright-orange fluorescence with a maximum emission wavelength of 578 and 572 nm, respectively, which correspond to the onset of the $\pi-\pi^*$ transition of the electronic absorption spectrum (Figure S6).

In the film state, the $\lambda_{max}$ values of P3PhT and P3PyT are bathochromically shifted to 458−555 and 461−539 nm, respectively, compared to those in the solution state (Figure 9). Furthermore, both polymers reveal a shoulder at 613 nm, which is related to a vibronic absorption. The observation of the bathochromic shifts and vibronic absorption peaks indicates that the $\pi$-conjugation lengths of both P3PhT and P3PyT are enhanced in the film state. Taking into account the structural analysis results discussed earlier, the enhanced $\pi$-conjugation lengths in both polymer films are attributed to the well-developed multilayer structures composed of laterally stacked backbone chains as one of the two sublayers (Figure 7). Moreover, onsets of the absorption band of P3PhT and P3PyT shifted to a wavelength longer than that of P3HT, which lead to the low-energy band gaps, as we expected.

**Table 3. HOMO and LUMO Levels of Polythiophene Derivatives**

| run | HOMO[a] (eV) | LUMO[b] (eV) | $\Delta E_{g,opt}$[c] (eV) |
|---|---|---|---|
| P3PhT | −5.17 | −3.42 | 1.75 |
| P3PyT | −5.38 | −3.57 | 1.81 |
| P3HT | −4.93 | −3.05 | 1.88 |

[a] Calculated by the equation HOMO $= -e(E^{OX}_{onset} - E^{1/2}_{ferrocene} + 4.8)$ (eV). [b] Calculated by the equation LUMO = HOMO + energy band gap (eV). [c] Calculated from onset wavelengths in UV−vis spectroscopy.

The energy band gap and HOMO/LUMO levels of P3PhT and P3PyT were determined by UV−vis spectroscopy (Figure 9) and CV analysis (Table 3 and Figure S7). These analyses found that P3PhT and P3PyT show lower HOMO levels than P3HT. The HOMO level decreases in the order of P3HT > P3PhT > P3PyT, which is coincident with the order of the electron densities of the thiophene units having hexyl, dimethyloctoxyphenyl, and dimethyloctoxypyridinyl side groups. In addition, P3PhT and P3PyT showed lower energy band gaps (1.75 and 1.81), respectively, than P3HT (1.88) because of their longer $\pi$-conjugation length due to their well-developed multilayer structures. These deeper HOMO levels and low band gaps of P3PhT and P3PyT would be suitable as *p*-type conjugated polymers for PSCs.

## Conclusions

Thermally stable P3PhT and P3PyT were successfully synthesized by the GRIM polymerization. The NMR and chromatography analyses confirmed that both polymers have a high regioregularity and low PDI. The DSC analysis found that P3PhT is crystalline while P3PyT is amorphous. However, the GIWAXS analysis indicated that both polymers reveal similar multilayer structures whose layers are stacked normal to the film plane. For the multilayer structures, each lamella consists of two sublayers, namely ordered and amorphous layers. There is no interdigitation between the adjacent layers. For both polymers, the aliphatic bristles always form an amorphous sublayer. However, the phenyl linker in P3PhT is excluded from the amorphous sublayer and, instead, included into the ordered sublayer because of its coplanarity with the thiophene backbone unit, whereas the pyridinyl linker is included in the amorphous sublayer because of its less coplanarity from the thiophene backbone unit. Thus, in the film, P3PhT forms an ordered sublayer with a relatively high

degree of order and large thickness compared to P3PyT. Such a high degree of order in the ordered sublayer is clearly reflected in the DSC thermogram, showing a $T_m$. In contrast, P3PyT shows no discernible melting transition in the DSC thermogram, indicating that the degree of order in the ordered sublayers of P3PyT is low. Consequently, P3PhT reveals a relatively longer $\pi$-conjugation length along the polymer backbone compared to P3PyT. However, P3PyT was confirmed to still have a relatively longer $\pi$-conjugation length along the polymer backbone in comparison to that of P3HT based on optical and electronic property analyses. These structural characteristics, in particular the enhanced $\pi$-conjugation length along the polymer backbone, are directly reflected in the optical and electronic properties, showing that both P3PhT and P3PyT exhibit a lower HOMO level and lower energy band gap compared to those of P3HT. These improved optical and electronic properties would be suitable for the fabrication of high-performance PSCs. In summary, the structure and properties of P3PhT and P3PyT make them promising materials for advanced PSCs with an excellent performance.

**Acknowledgment.** This work is partially supported by Japan Science and Technology Agency (JST) PRESTO program. This work was also supported in part by Global COE Program, Education and Research Center for Material Innovation, MEXT, Japan and Research Fellowships of the Japan Society for the Promotion of Science for Young Scientists. M.R. acknowledges the financial support of the National Research Foundation of Korea (Center for Electro-Photo Behaviors in Advanced Molecular Systems (2010-0001784) and of the Ministry of Education, Science & Technology (MEST) (BK21 Program and World Class University Program (R31-2008-000-10059-0). The synchrotron X-ray scattering measurements at Pohang Accelerator Laboratory were supported by MEST, POSCO, and POSTECH Foundation.

**Supporting Information Available:** $^1$H NMR and $^{13}$C NMR spectra of the monomers and fluorescence spectra of P3PhT and P3PyT. This material is available free of charge via the Internet at http://pubs.acs.org.

## References and Notes

(1) Pei, Q.; Yu, G.; Zhang, C.; Yang, Y.; Heeger, A. J. *Science* **1995**, *269*, 1086–1088.
(2) Murphy, A. R.; Fréchet, J. M. J. *Chem. Rev.* **2007**, *107*, 1066–1096.
(3) Zaumseil, J.; Sirringhaus, H. *Chem. Rev.* **2007**, *107*, 1296–1323.
(4) Burroughes, J. H.; Jpnes, C. A.; Friend, R. H. *Nature* **1988**, *335*, 137–141.
(5) Yu, G.; Heeger, A. J. *J. Appl. Phys.* **1995**, *78*, 4510–4515.
(6) Cheng, Y. J.; Yang, S. H.; Hsu, C. S. *Chem. Rev.* **2009**, *109*, 5868–5923.
(7) Osaka, I.; McCullough, R. D. *Acc. Chem. Res.* **2008**, *41*, 1202–1214.
(8) Ma, W.; Yang, C.; Gong, X.; Lee, K.; Heeger, A. J. *Adv. Funct. Mater.* **2005**, *15*, 1616–1622.
(9) Scharber, M. C.; Muhlbacher, D.; Koppe, M.; Denk, P.; Waldauf, C.; Heeger, A. J.; Brabec, C. J. *Adv. Mater.* **2006**, *18*, 789–794.
(10) Pei, Q.; Järvinen, H.; Österholm, J. E.; Inganäs, O.; Laakso, J. *Macromolecules* **1992**, *25*, 4297–4301.
(11) Haba, O.; Hayakawa, T.; Ueda, M.; Kawaguchi, H.; Kawazoe, T. *React. Funct. Polym.* **1998**, *37*, 163–168.
(12) Ouhib, F.; Hiorns, R. C.; Bailly, S.; Bettignies, R.; Khoukh, A.; Preud'homme, H.; Desbrie'res, J.; Dagron-Lartigau, C. *Eur. Phys. J. Appl. Phys.* **2007**, *37*, 343–346.
(13) (a) McCullough, R. D. *Adv. Mater.* **1998**, *10*, 93–116. (b) Loewe, R. S.; Ewbank, P. C.; Liu, J.; Zhai, L.; McCullough, R. D. *Macromolecules* **2001**, *34*, 4324–4333. (c) Iovu, M. C.; Sheina, E. E.; Gil, R. R.; McCullough, R. D. *Macromolecules* **2005**, *38*, 8649–8656.
(14) Yokoyama, A.; Miyakoshi, R.; Yokozawa, T. *Macromolecules* **2004**, *37*, 1169–1171.
(15) Miyakoshi, R.; Yokoyama, A.; Yokozawa, T. *J. Am. Chem. Soc.* **2005**, *127*, 17542–17547.
(16) Li, W.; Nelson, D. P.; Jensen, M. S.; Hoerrner, R. S.; Cai, D.; Larsen, R. D.; Reider, P. J. *J. Org. Chem.* **2002**, *67*, 5394–5397.
(17) (a) Lee, B.; Park, Y.-H.; Hwang, Y. T.; Oh, W.; Yoon, J.; Ree, M. *Nature Mater.* **2005**, *4*, 147–150. (b) Lee, B.; Oh, W.; Hwang, Y.; Park, Y.-H.; Yoon, J.; Jin, K. S.; Heo, K.; Kim, J.; Kim, K.-W.; Ree, M. *Adv. Mater.* **2005**, *17*, 696–701.
(18) (a) Yoon, J.; Kim, K. W.; Kim, J.; Heo, K.; Jin, K. S.; Jin, S.; Shin, T. J.; Lee, B.; Rho, Y.; Ahn, B.; Ree, M. *Macromol. Res.* **2008**, *16*, 575. (b) Kim, G.; Park, S.; Jung, J.; Heo, K.; Yoon, J.; Kim, H.; Kim, I. J.; Kim, J. R.; Lee, J. I.; Ree, M. *Adv. Funct. Mater.* **2009**, *19*, 1631–1644. (c) Yoon, J.; Jin, S.; Ahn, B.; Rho, Y.; Hirai, T.; Maeda, R.; Hayakawa, T.; Kim, J.; Kim, K.-W.; Ree, M. *Macromolecules* **2008**, *41*, 8778–8784.
(19) (a) Ree, M.; Ko, I. S. *Phys. High Tech.* **2005**, *14*, 2–7. (b) Ree, M.; Nam, S. H.; Yoon, M.; Kim, B.; Kim, K.-R.; Kang, T.-H.; Kim, J.-Y.; Kim, K.-J.; Shin, T. J.; Lee, H.-S.; Park, S.-J.; Kim, N.; Lee, K.-B.; Ko, I.-S.; Namkung, W. *Synchrotron Radiat. News* **2009**, *22*, 4–12.
(20) Ohshimizu, K.; Ueda, M. *Macromolecules* **2008**, *41*, 5289–5294.
(21) (a) Lee, B.; Park, I.; Yoon, J.; Park, S.; Kim, J.; Kim, K.-W.; Chang, T.; Ree, M. *Macromolecules* **2005**, *38*, 4311–4323. (b) Lee, B.; Yoon, J.; Oh, W.; Hwang, Y.-T.; Heo, K.; Jin, K. S.; Kim, J.; Kim, K.-W.; Ree, M. *Macromolecules* **2005**, *38*, 3395–3405.
(22) (a) Yoon, J.; Jin, K. S.; Kim, H. C.; Kim, G.; Heo, K.; Jin, S.; Kim, J.; Kim, K.-W.; Ree, M. *J. Appl. Crystallogr.* **2007**, *40*, 476–488. (b) Yoon, J.; Lee, S. W.; Choi, S.; Heo, K.; Jin, K. S.; Jin, S.; Kim, G.; Kim, J.; Kim, K.-W.; Kim, H.; Ree, M. *J. Phys. Chem. B* **2008**, *112*, 5338–5349. (c) Takahashi, A.; Rho, Y.; Higashihara, T.; Ahn, B.; Ree, M.; Ueda, M. *Macromolecules* **2010**, *43*, 4843–4852.